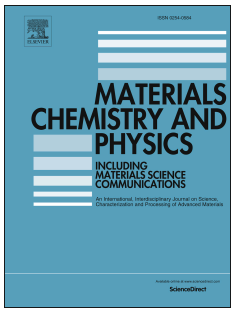

Controlled synthesis of mono- and bimetallic Pt-based catalysts for electrochemical ethanol oxidation

Natalia S. Veizaga, Gustavo Mendow, Andrés Felipe Quintero-Jaime, Ángel Berenguer-Murcia, Sergio de Miguel, Emilia Morallón, Diego Cazorla-Amorós

PII: S0254-0584(21)01065-8

DOI: https://doi.org/10.1016/j.matchemphys.2021.125282

Reference: MAC 125282

To appear in: *Materials Chemistry and Physics*

Received Date: 20 August 2021

Revised Date: 21 September 2021

Accepted Date: 23 September 2021

Please cite this article as: N.S. Veizaga, G. Mendow, André.Felipe. Quintero-Jaime, Á. Berenguer-Murcia, S. de Miguel, E. Morallón, D. Cazorla-Amorós, Controlled synthesis of mono- and bimetallic Pt-based catalysts for electrochemical ethanol oxidation, *Materials Chemistry and Physics* (2021), doi: https://doi.org/10.1016/j.matchemphys.2021.125282.

Natalia S. Veizaga: conceptualization, methodology, Investigation, data interpretation, Writing - original draft, Visualization

Gustavo Mendow: Investigation, Data curation, data interpretation, Writing - original draft.

Andrés Felipe Quinteros-Jaime: Investigation, data interpretation, Writing - original draft, Conceptualization, Visualization

Ángel Berenguer-Murcia: Investigation, Resources

Sergio De Miguel: Supervision, Resources, Writing - review & editing.

Emilia Morallón: Supervision, Resources, Writing - review & editing. Funding acquisition

Diego Cazorla-Amorós: Supervision, Resources, Writing - review & editing. Funding acquisition

CONTROLLED SYNTHESIS OF MONO- AND BIMETALLIC Pt-BASED CATALYSTS FOR ELECTROCHEMICAL ETHANOL OXIDATION.

Author 1 (Name, family name): Natalia Soledad, Veizaga[a, *]

Author 2 (Name, family name): Gustavo, Mendow[a],

Author 3 (Name, family name): Andrés Felipe, Quintero-Jaime[c],

Author 4 (Name, family name): Ángel, Berenguer-Murcia[b],

Author 5 (Name, family name): Sergio, De Miguel[a],

Author 6 (Name, family name): Emilia, Morallón[c],

Author 7 (Name, family name): Diego, Cazorla-Amorós[b]

[a] Instituto de Investigaciones en Catálisis y Petroquímica "Ing. José Miguel Parera" (INCAPE), Facultad de Ingeniería Química (UNL)-CONICET. 3000 Santa Fe, Argentina.

[b] Departamento de Química Inorgánica and Instituto Universitario de Materiales, Universidad de Alicante, Ap. 99, 03080, Alicante, Spain

[c] Departamento de Química Física and Instituto Universitario de Materiales, Universidad de Alicante, Ap. 99, 03080, Alicante, Spain

*Corresponding author: nveizaga@fiq.unl.edu.ar

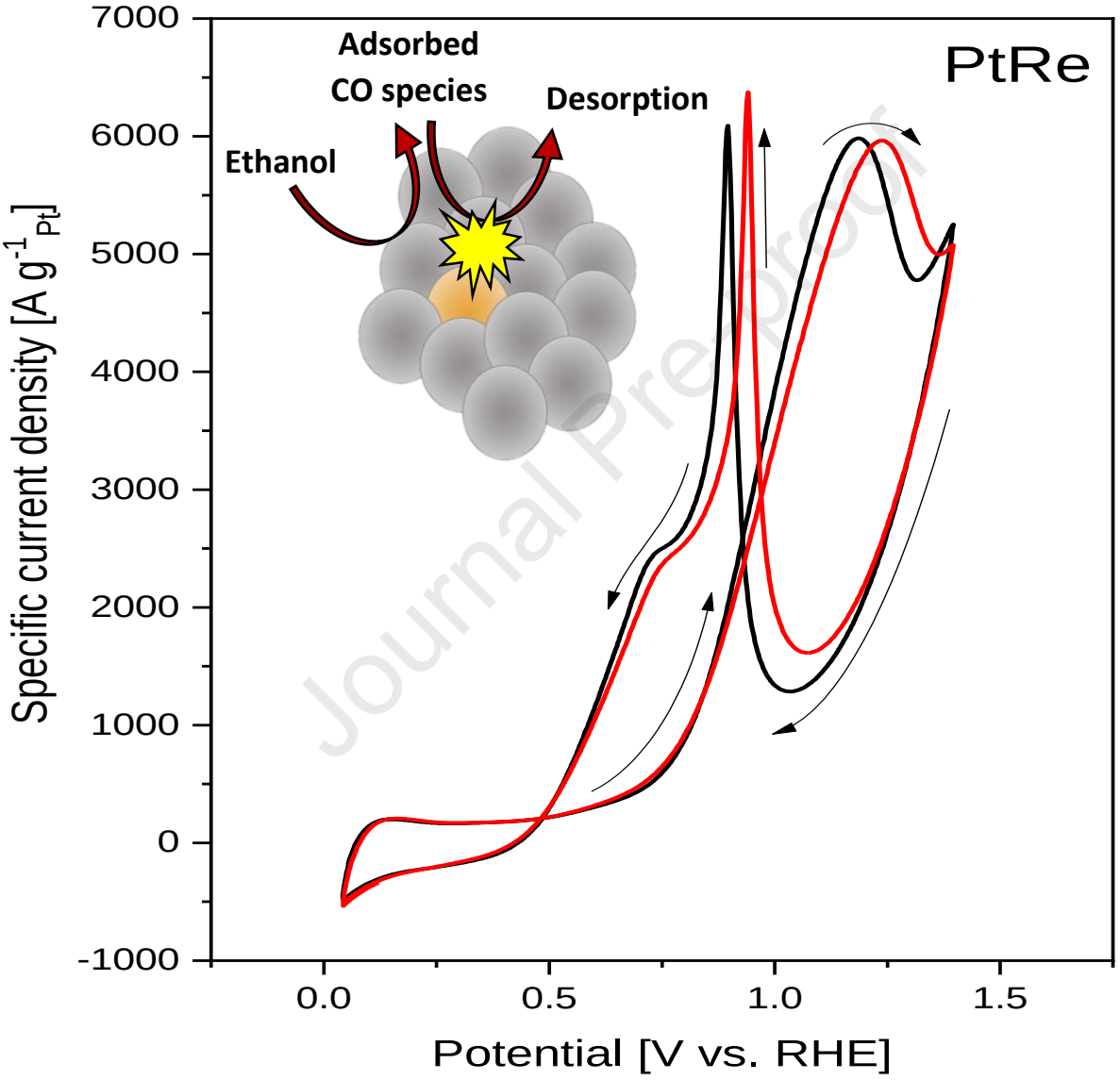

CONTROLLED SYNTHESIS OF MONO- AND BIMETALLIC Pt-BASED CATALYSTS FOR ELECTROCHEMICAL ETHANOL OXIDATION.

Natalia S. Veizaga[a], Gustavo Mendow[a], Andrés Felipe Quintero-Jaime[c], Ángel Berenguer-Murcia[b], Sergio de Miguel[a], Emilia Morallón[c], Diego Cazorla-Amorós[b]

[a] Instituto de Investigaciones en Catálisis y Petroquímica "Ing. José Miguel Parera" (INCAPE), Facultad de Ingeniería Química (UNL)-CONICET. 3000 Santa Fe, Argentina.

[b] Departamento de Química Inorgánica and Instituto Universitario de Materiales, Universidad de Alicante, Ap. 99, 03080, Alicante, Spain

[c] Departamento de Química Física and Instituto Universitario de Materiales, Universidad de Alicante, Ap. 99, 03080, Alicante, Spain

Abstract:

Poisoning tolerance of Pt-based catalyst is an important parameter for the designing of direct electrochemical fuel cells (EFCs) based on electrooxidation of alcohols (i.e. methanol, ethanol). Applicability of direct ethanol EFCs is still challenging taking into account the lack of effective electrocatalysts which are able to produce high faradic current densities and high stability towards strong adsorption of C1 and C2 oxidation products. As we present here, mono- and bimetallic Pt-based electrocatalysts have been synthesized on a carbon black support for the elecotrooxidation of ethanol in acidic media. Depending of the molar ratio between poly-n-vinylpyrrolidone (PVP, acting as protecting agent) and Pt, nanoparticle size distribution has been controlled, obtaining an optimal condition of Pt loading and electroactive surface area (ECSA) for the PVP/Pt ratio = 1. The electrochemical behavior of electrocatalyst Pt/Re/CB-1 shows a negligible variation in the ECSA (98.3 m^2 g^{-1}) in comparison with the monometallic electrodes (90.2 m^2 g^{-1}). In contrast, addition of Ir tends to reduce the ECSA by agglomeration of some nanoparticles and decreasing its electrochemical performance. Incorporation of Re in the alloy promotes bond breaking of the intermediates adsorbed on surface, specifically adsorbed C2 molecules, releasing great number

of the active sites from the Pt surface, minimizing the deactivation with cycling and providing remarkable stable catalyst with high specific current densities with the addition of small amounts of Re.

Keywords: platinum, electrocatalyst, ethanol oxidation, iridium, rhenium

1. Introduction

Fuel Cells (FCs) have received significant attention as a promising environmentally sustainable technology for energy generation, complementary to the current non- and renewable source of energy, helping to supply the current global energy demand. In this sense, hydrogen has been considered as the best fuel option, taking into account its abundance, easy production by fuel reforming or water electrolysis and the products generated in the FC [1,2]. Unfortunately, the issues related with hydrogen storage limits its applicability in different fields (e.g. automobile). Therefore, other alternatives for suitable fuels to be used directly in fuel cells, have been extensively investigated [3,4]. Among them, the use of organic fuels, specifically methanol, have provided an interesting alternative for energy production, despite their low electrochemical activity and kinetics, in comparison with hydrogen[4].

Methanol presents high availability, easy storage and low price; however, important concerns about its toxicity in human beings is still critical for its application. In this sense, previous studies in FCs have demonstrated outstanding output energy density values of around 8.0 kWh kg^{-1} employing ethanol, in comparison with the values obtained for methanol of 6.1 kWh kg-1 [5,6]. In addition, low toxicity and easy production from biomass turns this C-2 type alcohol into a highly promising candidate to be employed in FCs as a replacement of methanol. Platinum-based catalysts have provided very high oxidizing features to make up for the low activity of ethanol, facilitating the C-C breakdown [7,8]. Nevertheless, the high tendency towards the formation of C1 or C2 intermediates on the Pt surface, which block the active sites of the Pt surface, tends to reduce the electroactivity by catalyst poisoning [9]. One interesting and widely accepted strategy to enhance the catalytic activity has been developed by using multifunctional electrocatalysts, combining Pt with other metals (e.g. Ru, In, Ge, Sn) [10–15]. Binary or ternary systems containing Pt produce a coverage of the catalyst surface with oxygenated Metal-OH species from water dissociation that facilitate the oxidation of the adsorbed intermediates [3,16]. Along this line, the use of Iridium and Rhenium has gained interest in recent years as alloying metal with Pt despite the low electrocatalytic activity towards oxidation reactions in comparison with the Pt alone [17–

19]. In this regard, computational studies have shown that the incorporation of Ir in Pt-based catalyst shows a decrease in the energetic barriers of C-C splitting [20]. Latest effect produces a remarkable enhancement in the electrocatalytic activity, observed in the high selectivity towards direct CO_2 production after the oxidation and a shift to lower potentials in the onset oxidation potential [17,21]. Indeed, recent studies performed by Chang et al. [22] have demonstrated that Ir-Pt monolayer alloy on Pt (100) nanocubes tends to produce a large amounts of CO_2 during the electrooxidation, decreasing the formation of C_xH_yO/C_xH_y species. Similar electrochemical behavior have been observed in Pt-SnO_2 electrocatalysts [23].

Following the same principle, Re incorporation into the Pt-based catalysts has been considered a good candidate to increase the kinetics of C-C bonds breakdown [24–26], in order to improve the catalytic activity of Pt-based catalysts towards ethanol oxidation to CO_2 and the poisoning tolerance, facilitating the C-C splitting of the C2 species adsorbed onto the electrocatalyst. Few works have properly reported the effect of Re in the electrochemical performance towards electrooxidation of alcohols. Tayal et al. [24] and Choudhary et al. [27] have proved that the incorporation of small amount of Re in a ternary system Pt-Sn-Re/C or Pt-Ru-Re/C decreases the onset potential to about 150-300 mV, obtaining the highest faradic current and the maximum power density. Besides, Drzymała et al. [28] have proved that the presence of Re in Pt/SnO_2-based electrocatalysts increases up to 4 time the specific activity as well as a negligible variation in the electrochemical surface area, proving highly cycling stability.

At this point, not only has the chemical composition of the catalyst been crucial to the proper performance, but also the properties and nature of the support, as well as the synthesis method, which are all gaining increasing relevance for electrocatalysts synthesis in the last years. For example, depending of the support employed high catalytic activity with low Pt loadings can be reached, associated with the 3D structure, higher surface area and high conductivity of the carbon material support [29].

Nowadays, a wide variety of reduction methods for Pt-based catalysts synthesis have been reported in the literature using different reduction agents such as hydrazine [30], sodium

borohydride [31], and thermal reduction with hydrogen [32,33]. However, good homogeneity, reducibility of the metal precursor, degree of loading and control over the morphology and nanoparticle size are still critical parameters in the synthesis of the catalyst. In this context, the synthesis of colloidal catalyst nanoparticles employing the reduction-by-solvent method employing ethylene glycol [34], combined with a suitable capping agent, have truly provided a preparation method in which nanoparticle size distribution and morphology can be readily controlled [35]. In fact, CO tolerance of the Pt nanoparticle can be substantially improved in comparison with a bulk Pt electrode [36]. This method has been extended for a wide variety of metal nanoparticles to be used in a large number of applications (e.g. dehydrogenation of formic acid [37], oxygen reduction reaction [38] or sensing applications [39,40]). In fact, reduction of the metal catalyst in presence of the carbon material support has offered a good distribution of the nanoparticles onto the support with high reproducibility and loading.

In this work, mono- and bimetallic Pt-based catalysts have been synthesized controlling the nanoparticle size and distribution onto a carbon black (CB) support, modifying the ratio between platinum precursor and protecting agent (PVP). The optimal conditions for platinum loading, nanoparticle size, highest value of electrochemical active surface area and stability towards ethanol oxidation for monometallic nanoparticles were obtained for a PVP/Pt ratio of 1. In this sense, Iridium and Rhenium precursors have been incorporated into the synthesis of the catalysts in order to produce bimetallic catalyst of Pt/Ir and Pt/Re alloys. Incorporation of the second metal shows a dependence with the presence of protecting agent during synthesis. It must be noted that incorporation of Re to the synthetic protocol has provided an important enhancement in the poisoning tolerance during ethanol oxidation compared to monometallic and Ir containing catalysts.

2. Experimental

2.1. Reagents and materials

Carbon black CD6008 employed as support for the catalysts preparation was provided by Columbian Chemicals Company (Brunswick, Ohio). Its specific surface area, determined by applying the Brunauer, Emmett and Teller (BET) method to the N_2 adsorption isotherm at 77K, is 605 m^2 g^{-1} and the mesopore volume was 0.38 cm^3 g^{-1} [37].

Nitric acid (65%) and hydrochloric acid (37%) were obtained from Panreac and VWR Chemicals, respectively. Acetone (99.8%) and absolute ethanol (EtOH, 99.5%) were obtained from Merck. All the solutions were prepared using ultrapure water (18 MΩ cm, Purelab Ultra Elga equipment). The gases (N_2 (99.999%) and H_2 (99.999%)) were supplied by Air Liquide.

Reagents employed for catalysts synthesis were hexachloroplatinic acid hydrate ($H_2PtCl_6 \cdot xH_2O$, 99.99%), Hexachloroiridium acid hydrate ($H_2IrCl_6 \cdot xH_2O$, 99.98%) and Perrhenic acid solution ($ReHO_4$, 75-80 wt. %). poly-n-vinylpyrrolidone (PVP, 40K), sodium hydroxide (NaOH, 99.99% purity) and anhydrous ethylene glycol (EG) were purchased from Sigma-Aldrich.

2.2. Synthesis of mono- and bimetallic catalyst

Monometalic and bimetallic Pt-based catalysts were synthesized following the reduction-by-solvent method [35], adapting a previously published procedure [41,42]. A typical synthesis step-wise procedure is described with details below (see Scheme 1).

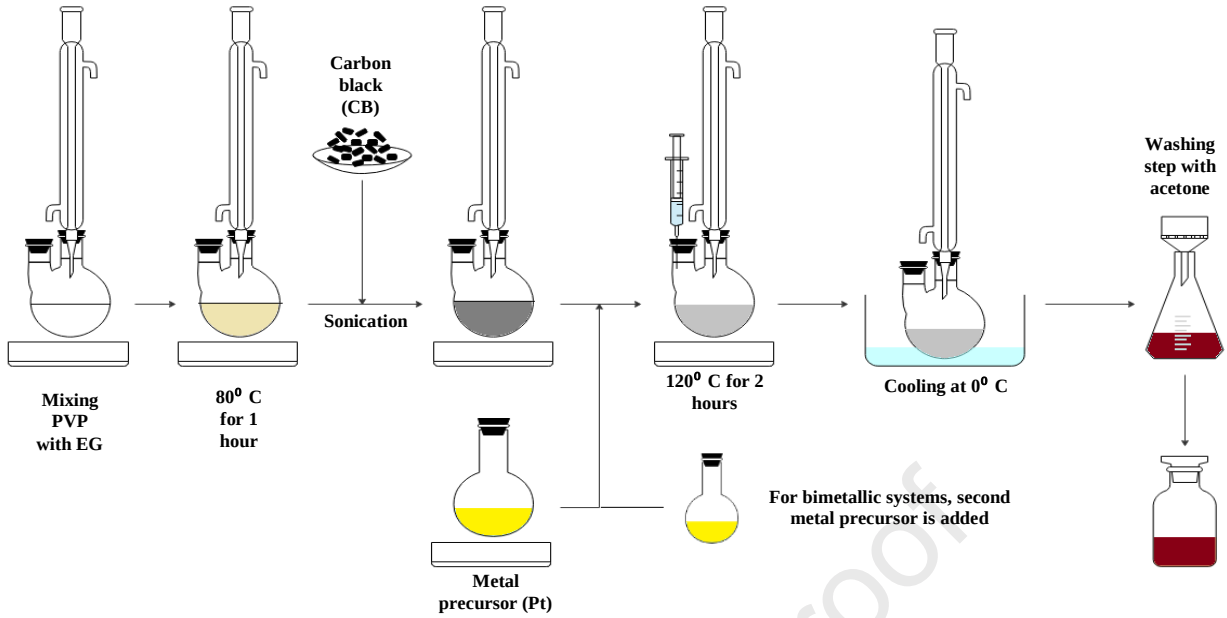

Scheme 1. Scheme of the mono- and bimetallic catalyst synthesis by the reduction-by-solvent method.

In a two-necked, round-bottom flask of 100 mL, the necessary amount of protecting polymer (PVP) was dissolved in a 3:1 (v:v) solution of ethylene glycol and water at 80ºC for 1 hour, under stirring conditions. Subsequently, 250 mg of the carbon support (CB) was incorporated into the solution and submitted to sonication for 30 minutes. Afterwards, 158 mg of platinum precursor was dissolved in the solution under reflux conditions for 2 hours at 120ºC, in order to deposit the metal nanoparticles directly on the carbon support [41]. During the synthesis of the catalyst inert argon atmosphere was employed, using a Schlenk system to avoid undesirable side reactions. The resulting solution was cooled down to 0ºC, filtered and washed with excess of water and acetone, to remove the remaining capping agent and different by-products generated. Taking into account that PVP in the reduction-by-solvent method controls the nanoparticle size and size distribution, different molar ratios PVP:Pt were evaluated (10, 2.5, 1, 0.1 and 0).

For bimetallic catalysts containing Ir and Re, the synthesis process was carried out under the same conditions as the monometallic catalyst. However, the second metal precursor 1.9 mL of 0.02 M $H_2IrCl_6 \cdot xH_2O$ or 5 mL of 0.02 M $ReHO_4$ for PtIr and PtRe electrocatalyst, respectively, was incorporated at the same time as the platinum precursor. In all cases, platinum loading was

fixed at 20 wt. %. The alloying metal loading was fixed at 5 wt. %. The selected PVP/Pt ratio for the bimetallic catalysts was 1. In the case of Pt/Re/CB catalyst, reduction was carried out by adding 160 mg sodium borohydride ($NaBH_4$), taking into account that ethylene glycol does not fully reduce the Re and Pt precursors [43,44]. Afterwards, different electrocatalysts have been dried under vacuum at 70ºC.

In this work, the electrodes prepared are named as Pt/CB-X for the monometallic catalyst prepared with Pt/CB-X, Pt/Ir/CB-X and Pt/Re/CB-X for the bimetallic catalysts. In both cases, X represents the PVP/Pt ratio employed during the synthesis.

2.3. Physico-chemical characterization

Transmission electron microscopic measurements (TEM) were carried out using a JEOL JEM-2010 model Transmission Electron Microscope equipped with an Oxford X-ray detector (EDS), INCA Energy TEM 100 model, and a GATAN acquisition camera. All electrocatalysts were suspended in isopropanol and deposited in a copper mesh until dry the solvent. TEM micrographs have been obtained using 200 kV acceleration voltage.

X-Ray photoelectron spectroscopy (XPS) was performed in a VG-Microtech Multilab 3000 spectrometer using Al Kα radiation (1253.6 eV), monochromatized by a twin crystal monochromator, yielding a focused X-ray spot (elliptical shape-400 μm) at 3 mA x 12 kV. The analyzer was operated in the constant energy mode with survey scan pass energies of 200 eV to measure the whole energy band and 50 eV in a narrow scan to selectively measure the particular elements. XPS data were analysed with Avantage software. A smart background function was used to approximate the experimental backgrounds and surface elemental composition were calculated from background-subtracted peak areas. Compensation of charge was performed with the system flood gun in order to provide low energy electrons and low energy argon ions from a single source.

The deconvolution of the XPS Pt4f, Ir4f and Re4f signals was done by least squares fitting using Gaussian-Lorentzian curves, while a Shirley line was used for the background

determination. Spectra of Pt4f, Ir4f and Re4f have been analyzed considering the spin-orbit splitting into $4f_{7/2}$ and $4f_{5/2}$ for all metal species. The spectra were deconvoluted considering a ratio of areas for $4f_{7/2}$ and $4f_{5/2}$ of 4:3 and an energy splitting of the spin orbit coupling for Pt4f, Ir4f and Re4f of 3.3, 3.0 and 2.4 eV respectively [45].

In order to determine the metal loading, 10 mg of the catalyst were digested in aqua regia (1 HNO_3 (65%):3 HCl (37%)). The suspension was sonicated for 20 minutes and heated at 80ºC for 6 hours until complete evaporation. Afterwards, 2 mL of HNO_3 were added, filtered and diluted with ultrapure water to a final volume of 100 mL. The solutions were then analyzed using inductively coupled plasma optical emission spectroscopy (ICP-OES) with a Perkin-Elmer Optima 4300 equipment with a power generator of 1300 W. Gas flow for plasma of 15 L min^{-1} and sample flow (liquid) of 1 mL min^{-1}). Iridium and Rhenium determination could not be performed using the previous sample treatment, therefore, quantification of the second metal was not possible by ICP.

2.4. Electrochemical characterization

The working electrode was prepared using a 1 mg mL^{-1} dispersions of the different metal catalysts, dispersed under sonication for 10 min in acetone and 0.02% wt% Nafion®. Prior to the deposition of the catalyst, the glassy carbon electrode surface (3 mm diameter) was sanded with emery paper and polished using 1 and 0.05 µm alumina slurries and then rinsed with ultrapure water. Afterwards, 10 µL aliquots of the dispersion were dropped onto the glassy carbon (GC) surface and dried under an infrared lamp to remove the solvent. The procedure was repeated 4 more times in order to deposit a theoretical amount of 40 µg of the catalyst on the electrode.

Electrochemical characterization was performed by cyclic voltammetry in 0.5 M H_2SO_4 solution, using an eDAQ Potentiostat (EA163 model) coupled to a wave generator (EG&G Parc Model 175) and the data acquisition was done with an eDAQ e-corder 410 unit (Chart and Scope Software), using a standard three-electrode cell configuration. The glassy carbon electrode modified with the metal catalyst was used as the working electrode (WE), a platinum wire was

used as counter electrode (CE) and a reversible hydrogen electrode (RHE) introduced in the same electrolyte was the reference electrode (RE). Different catalyst electrodes were submitted to 20 cycles at 50 mV s^{-1} by cyclic voltammetry under inert atmosphere and room temperature.

2.4.1. CO-stripping test

For CO-stripping, the electrocatalysts have been polarized for 180 min at a potential of 0.4 V vs. RHE in a CO-saturated solution of 0.5 M H_2SO_4. Then, N_2 was passed to purge the non-adsorbed CO in the electrolytic.

In order to determine the electroactive Pt surface area (ECSA) in the different electrocatalyst synthesized, the estimation was carried out by integration of the charge of the desorption process of the CO in the 0.5 M H_2SO_4, N_2-saturated, using the following equation:

$$ECSA = \frac{Q}{4.2 m_{Pt}} \qquad \text{Eq. 1.}$$

Where ECSA is in $m^2\ g^{-1}$; Q is the charge in C, m_{Pt} is the mass of platinum in g and 4.2 C m^{-2} corresponds to the theoretical charge charge of monolayer CO surface coverage in Pt. In the case of catalysts prepared with a PVP/Pt ratio of 10, no evidence of Pt oxide redox processes made the determination of ECSA unfeasible in these catalysts.

2.4.2. Electrocatalytic behaviour towards ethanol oxidation

Electrocatalytic activity towards ethanol oxidation was evaluated by cyclic voltammetry, using the same electrochemical cell configuration with three electrodes described in above in previous section. The catalysts deposited on the glassy carbon electrode (working electrode) were submitted to continuous cycling at 20 mV s^{-1} under inert atmosphere in a solution of 0.5 M H_2SO_4 and 1 M ethanol in a potential range between 0.04 to 1.4 V vs. RHE.

Stability test has been performed by chronoamperometry submitting the electrocatalyst to a fixed potential of 1.0 V for 180 min in 0.5 M H_2SO_4 + 1 M EtOH for 180 min.

3. Results and Discussion

3.1. Optimization of the Pt/CB catalyst: Characterization of monometallic Pt-based catalyst.

Platinum loading in the catalysts was quantified by ICP-OES as shown in Table 1. Concentration of Pt in the catalyst shows a dependence with the PVP/Pt ratio employed during the synthesis, obtaining loadings close to the theoretical value of 20 wt. % at lower PVP concentrations (PVP/Pt ratios of 0 and 0.1). The effect of PVP/Pt ratio in the amount of Pt in the catalysts was previously studied by other authors but only ratios lower than 1 were used [46]. A decrease in the Pt concentration is observed at PVP/Pt ratios >1 which can be explained by a hindrance effect between the PVP capping agent and the nanoparticles surface which does not allow interactions between nanoparticles and the carbon support, as it has been reported recently [46,47]. Under these conditions, anchoring and adsorption of the Pt nanoparticles on the CB surface are not favored and then, some Pt nanoparticles that are stabilized by the PVP polymer may just remain in the solution.

Table 1. Platinum loading obtained by ICP, nanoparticle size by TEM and chemical composition of the Pt species by XPS.

Pt/CB catalyst	d_{TEM} [nm]	Pt wt. % ICP	Pt wt. % XPS
Pt/CB-0	12.74 ± 8.61	18.3	10
Pt/CB-0.1	4.37 ± 2.52	18.8	12
Pt/CB-1	2.96 ± 0.56	12.5	13
Pt/CB-2.5	3.30 ± 0.63	9.7	8
Pt/CB-10	2.58 ± 0.71	1.6	4

XPS spectra for Pt4f core level region for the different synthesized catalysts in Figure 1 show that Pt nanoparticles present two main peaks which can be deconvoluted mainly into two doublets at binding energies of 71.5 and 74.8 eV associated with Pt0 species and 72.8 and 76.1 eV related with oxidized platinum species (Pt^{2+}), the latter being generated by surface oxidation of the Pt nanoparticles in the presence of water during the synthesis and possible interactions with the PVP

adsorbed onto the Pt surface [48,49]. Furthermore, the Pt^0/Pt^{2+} ratios for all the different catalysts synthesized is *ca* 3.2; thus, the PVP amount does not seem to affect the chemical nature of the surface of Pt in the catalyst.

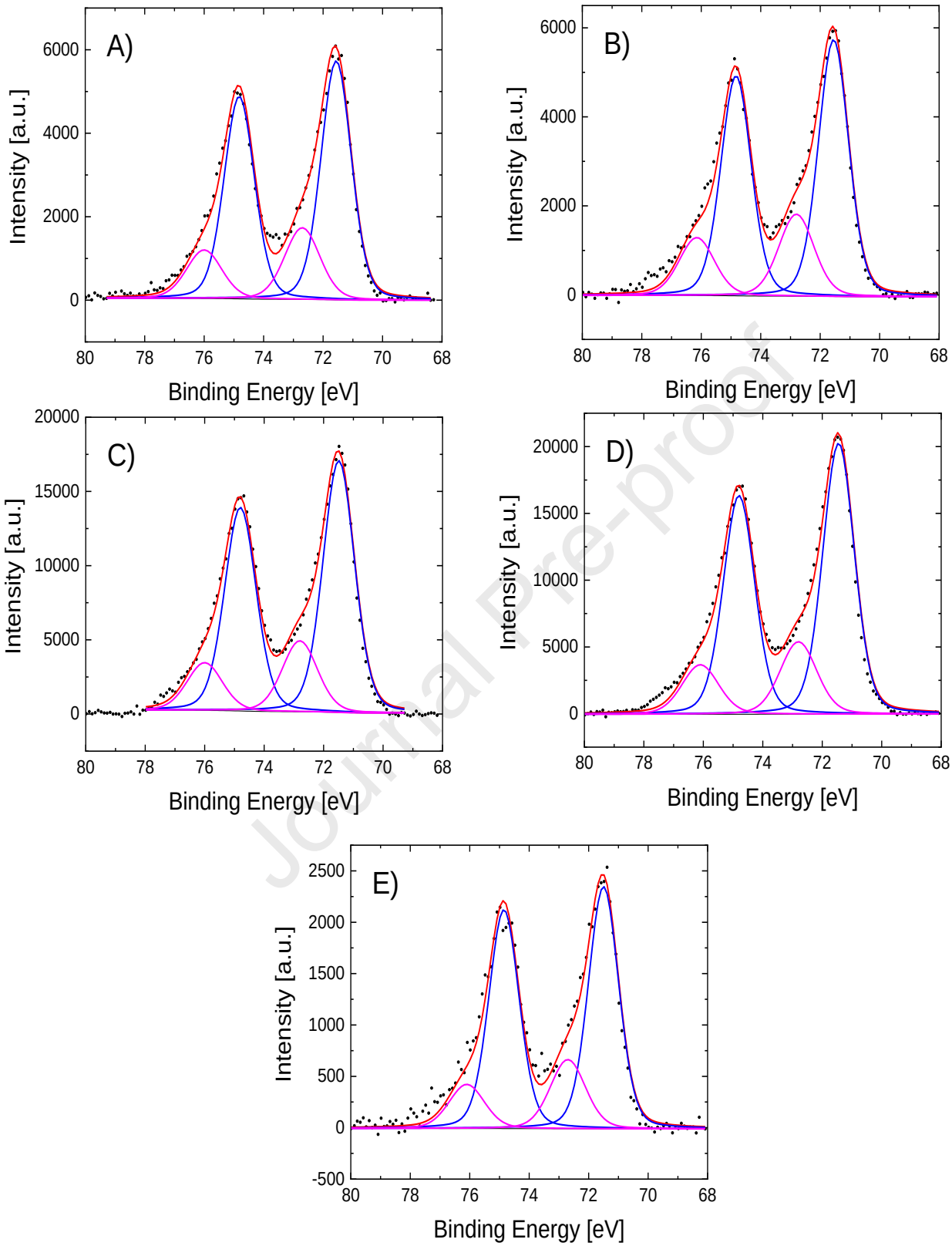

Figure 1. Pt4f XPS spectra for different Pt/CB catalysts synthesized with different PVP/Pt ratios: A) 0, B) 0.1, C) 1, D) 2.5 and E) 10.

Morphological characterization by TEM in Figure 2 of the Pt/CB catalyst synthesized with different PVP/Pt ratios shows a good distribution of the Pt nanoparticles on the carbon black support.

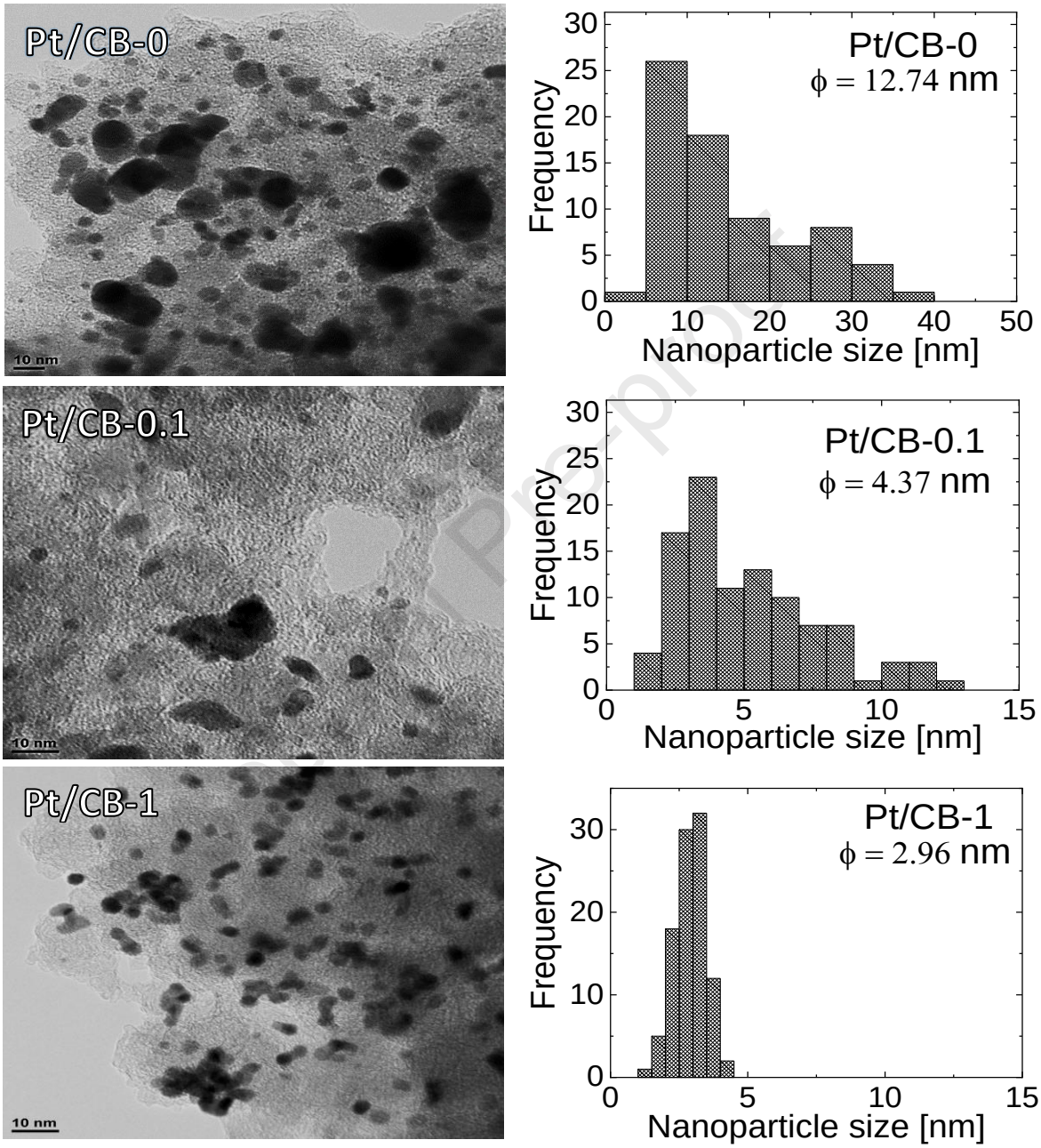

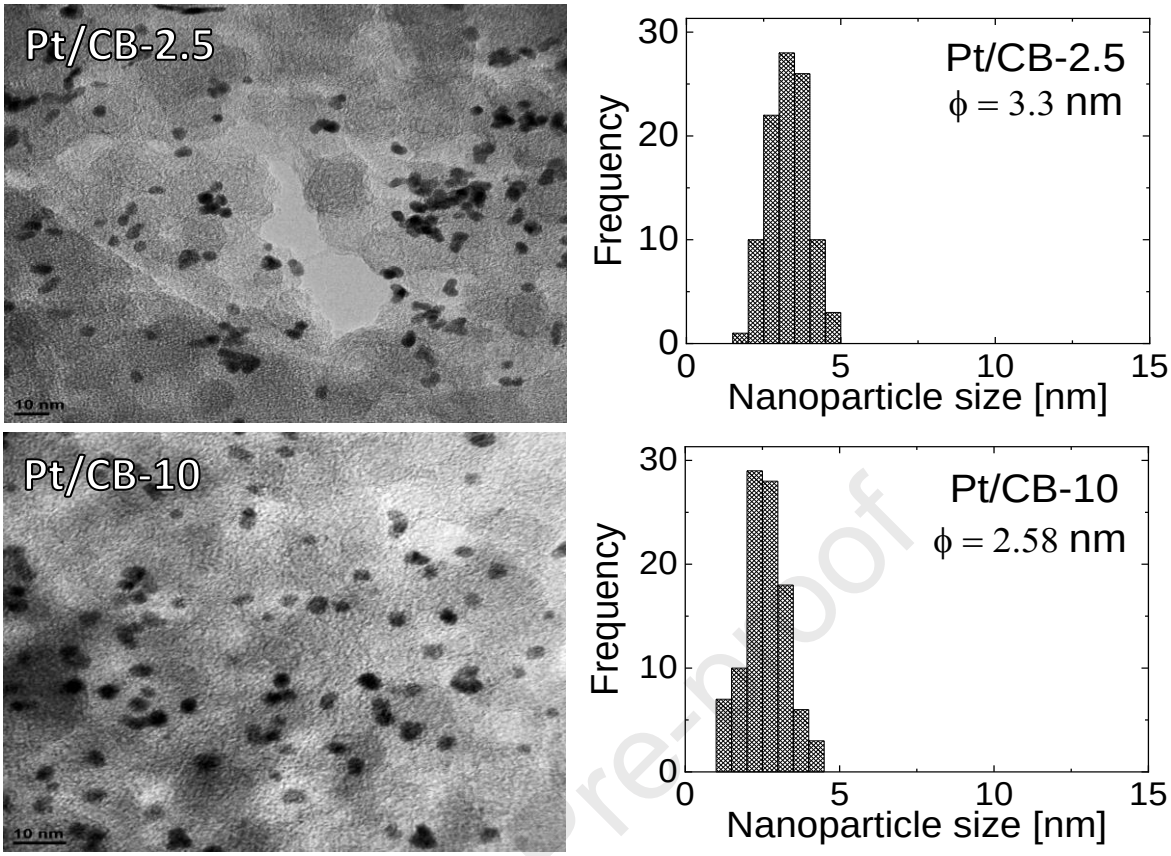

Figure 2. TEM micrographs of the Pt/CB catalyst synthetized with different PVP/Pt ratios.

Depending of the PVP employed during the synthesis, different nanoparticle size distribution has been obtained in the catalyst. In the case of the catalysts prepared in absence of PVP, a wide nanoparticle size distribution with an average nanoparticle size of around 12.74 nm and non-spherical morphology is observed, as a consequence of the coalescence of the nanoparticles and further agglomeration during the synthesis. On the other hand, catalysts synthesized in the presence of PVP show a narrow distribution of the nanoparticle size, which also involves a reduction of the nanoparticle size, as it has been previously reported [46,50,51]. Interestingly, platinum nanoparticles in samples with PVP/Pt ratios of 1, 2.5 and 10 show narrower nanoparticle size distributions with average size values of 2.96, 3.30 and 2.58 nm, respectively (see Figure 2 inset).

Figure 3 shows the steady state voltammograms of Pt/CB electrodes in acidic conditions (0.5 M H_2SO_4) normalized to the platinum loading and the CO-stripping cyclic voltammograms (Inset).

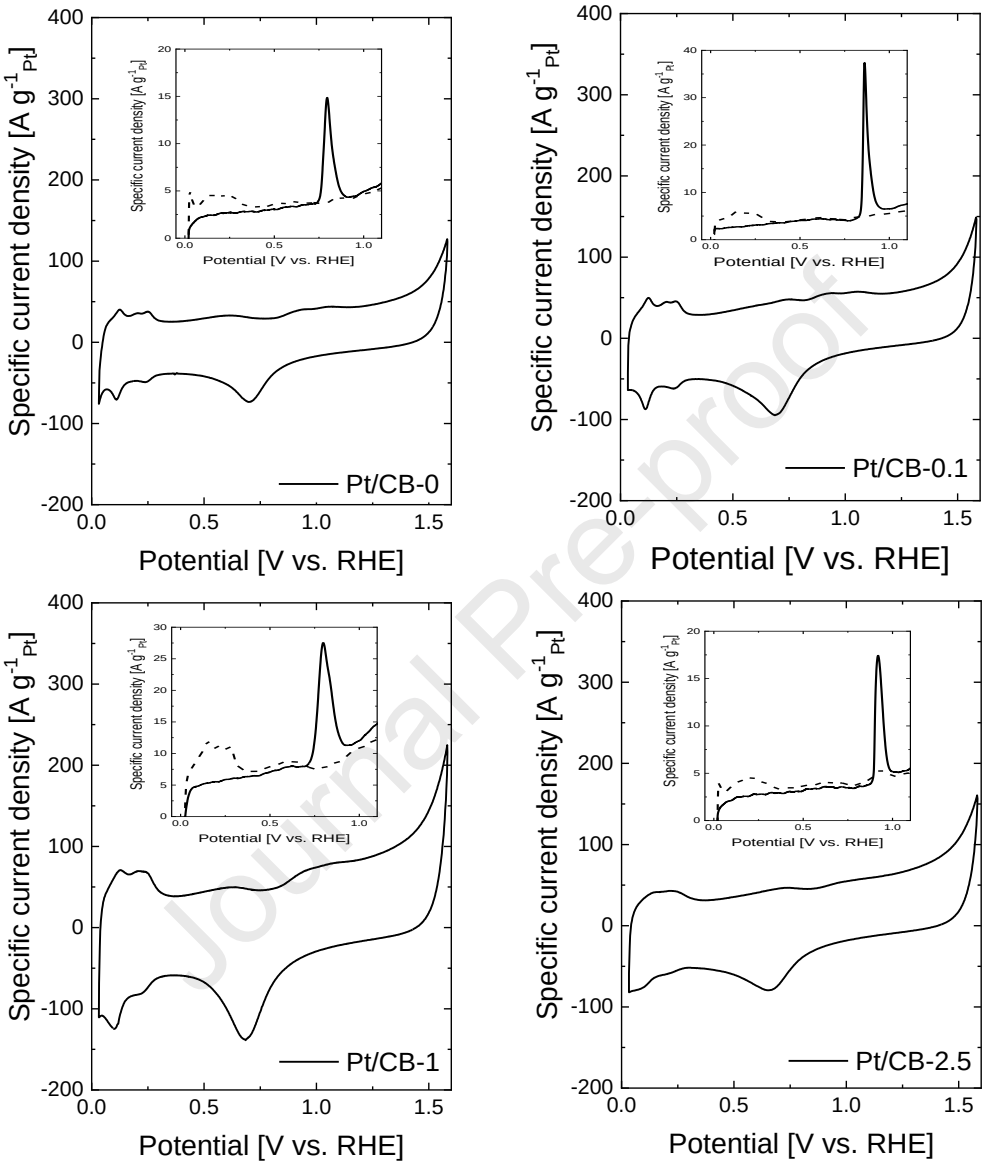

Figure 3. Cyclic voltammograms of Pt/CB catalyst synthesized with different PVP/Pt ratios in 0.5 M H_2SO_4 at 50 mV s^{-1} under inert atmosphere. Inset: CO-stripping profiles performed in 0.5 M H_2SO_4 at 25 mV s^{-1}.

Cyclic voltammograms in acid media show that the catalysts prepared with PVP/Pt ratios below 2.5, present the hydrogen adsorption–desorption peaks in the potential range of 0.06–0.4 V vs. RHE, consistent with processes on Pt electrode. Higher PVP/Pt ratios during the synthesis

tend to produce a blocking of the hydrogen process as it has been observed in samples with PVP/Pt ratio of 10. Therefore, excess capping agent is adsorbed on the Pt nanoparticles surface. In fact, the catalyst prepared with a PVP/Pt ratio of 10 (see Figure S1-A) does not show the voltammetric profile characteristic of Pt. Thus, excess PVP blocks the Pt nanoparticle surface. Additionally, the redox couple at around 1.03/0.68 V related with the platinum oxide formation, shows a direct dependence with the PVP/Pt ratio employed, which is consistent with the amount of Pt obtained by ICP. Nevertheless, the catalyst prepared with a PVP/Pt ratio of 1 shows the most important contribution in charge related with the Pt oxide reduction, despite having a lower loading than the catalyst prepared with 0.1 and 0 ratios. This latest statement can be attributed to the presence of small Pt nanoparticles with a narrow size distribution, which generates the highest electroactive surface area (see below) [52,53].

CO-stripping profiles (see Figure 3-Inset) show that the onset potential (E_{onset}^{CO}), as well as, the peak potential (E_p^{CO}) of the CO-desorption varies with the PVP/Pt ratio. In this regard, lowest values of E_{onset}^{CO} and E_p^{CO} are observed in electrocatalyst with PVP/Pt = 1 at around 0.7 and 0.8 V vs. RHE, which are lower to the CO stripping for commercial Pt-Vulcan electrocatalyst to about 0.86 V reported in literature [54]. In contrast, increasing of PVP concentration produces a positive shifting to higher potential of 130 mV and decreasing of the catalytic activity towards the oxidation of the CO, which can be related with the low Pt loading obtained in this electrocatalyst [55].

Regarding ECSA, Table 2 shows that the catalyst prepared with a PVP/Pt ratio of 1 presents the highest value of electroactive surface area, which agrees with the small nanoparticle size obtained. This value is similar to that previously obtained with Vulcan XC-72R as support [43], obtained from the CO-stripping profiles.

Table 2. Values of ECSA and Pt nanoparticle size for the Pt/CB catalyst prepared with different PVP/Pt ratios.

Pt/CB catalyst	ECSA [$m^2\ g^{-1}$]	d [nm]$_{ECSA}$	E_{onset} [V]	I_f [A g_{Pt}^{-1}]*	I_f/I_b*
Pt/CB-0	32.3	8.7	0.51	361.5	0.93
Pt/CB-0.1	59.1	4.7	0.50	396.3	0.91
Pt/CB-1	90.2	3.1	0.48	470.7	1.07
Pt/CB-2.5	59.7	4.7	0.73	317.9	1.40
Pt/CB-10	--	--	--	--	--

*I_f: current density in the forward wave. I_b: current density in the backward wave.

3.2. Electrocatalytic activity for ethanol oxidation reaction of monometallic catalyst

The electrocatalytic activity of the different Pt/CB catalysts was performed in ethanol oxidation in acid media (0.5 M H_2SO_4 + 1 M EtOH) as shown in Figure 4.

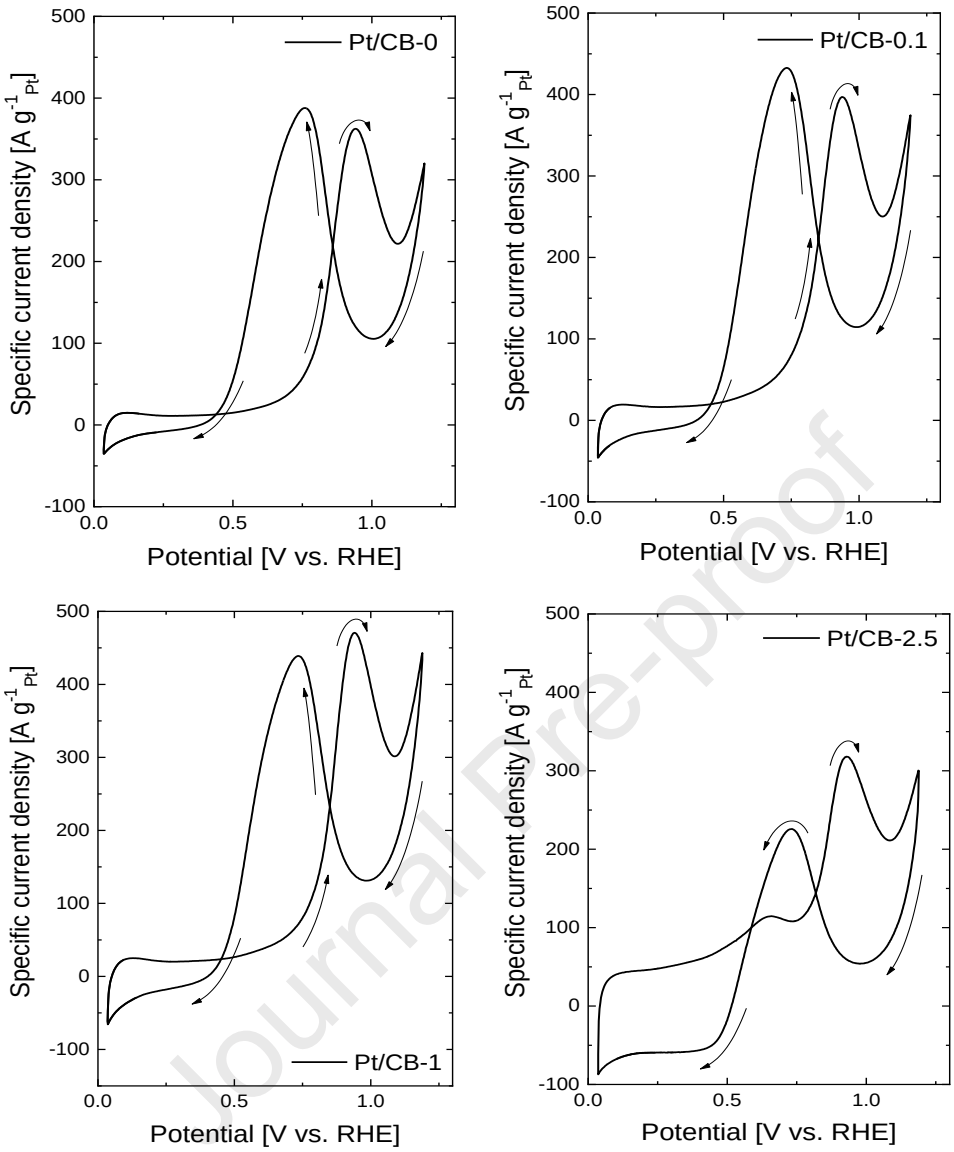

Figure 4. Cyclic voltammograms of Pt/CB catalyst synthesized with different PVP/Pt ratios in 0.5 M H_2SO_4 + 1 M EtOH at 20 mV s^{-1} under inert atmosphere (cycle: 20).

The voltammograms show for all catalysts during the positive scan an irreversible oxidation peak associated with ethanol oxidation and the oxidative desorption of the intermediates. During the reverse scan an oxidation peak is also observed associated also to ethanol oxidation. However, depending of the PVP concentration, different electrochemical behaviors are observed. Samples with PVP/Pt ratios of 2.5 and 10 show a lower catalytic activity, as a direct consequence of the partial blocking of the active sites in the Pt nanoparticles by the adsorbed PVP (See Figure 4-D and Figure S1-B). Additionally, those catalysts might present low poisoning tolerance and high

tendency towards poisoning after ethanol oxidation. Therefore, accumulation of carbonaceous species may be more favorable in those catalysts [56]. This is clearly observed in the ratio between forward current and reverse current that deviates from the unity with the PVP/Pt ratio (Table 2).

In contrast, in the electrodes prepared with small PVP/Pt ratios, the active sites are more exposed to the medium. All catalysts show maximum peak potentials of the forward and reverse oxidation peaks at around 0.94 and 0.73 V, respectively. Interestingly, Pt/CB-1 catalyst shows a combination of Pt loading and average nanoparticle size (2.96 nm) which provides an optimal value where a high catalytic response is obtained, which can be understood considering the highest values of ECSA obtained. However, upon cycling, there is a clear decrease in activity (see Figure S2) due to accumulation of reaction intermediates which is detrimental from an application point of view.

Taking into account that Pt/CB-1 catalyst shows the highest electrocatalytic activity towards electrooxidation of ethanol with small nanoparticle size distribution and low platinum loading (see Figure S3), the synthesis of the subsequent bimetallic catalysts was performed and evaluated with this PVP/Pt ratio. Additionally, bimetallic catalysts with no PVP (PVP/Pt ratio of 0) were also synthesized for comparative purposes.

3.3. Bimetallic catalyst characterization and electrochemical performance

XPS analysis for the bimetallic catalysts presented in Table 3 indicates that the presence of PVP tends to produce higher Ir and Re loadings into the Pt nanoparticles, in comparison with the samples prepared without PVP, suggesting that stabilization of the alloying phase in Pt/Ir/CB and Pt/Re/CB is promoted by the presence of the capping agent. However, nominal values of the second metal are lower than the chosen theoretical values (see Figure S4). Taking into account that the lack of PVP results in a negligible incorporation of Ir and Re in the bimetallic catalysts, the following results correspond to the bimetallic catalyst obtained with PVP/Pt ratio of 1.

Table 3. Compositional analysis of the bimetallic catalyst (Pt/Ir and Pt/Re) prepared with PVP/Pt ratio of 0 and 1.

Bimetallic catalyst	Pt %wt XPS	$\%Pt^0$	$\%Pt^{2+}$	Ir %wt XPS	Re %wt XPS
Pt/Ir/CB-0	8	83	18	1.8	--
Pt/Ir/CB-1	12	82	19	3	--
Pt/Re/CB-0	5.5	79	21	--	0.29
Pt/Re/CB-1	8	74	26	--	2.1

XPS spectra for Pt4f shows two main contributions associated with the presence of Pt^0 and Pt^{2+} at binding energies of around 71.5 and 72.8 eV for both bimetallic catalysts, suggesting the stabilization of metallic platinum and the oxidized species. In the case of Pt/Re/CB-1 catalyst a higher stabilization of more oxidized species seems to occur, in agreement with other different Pt alloys-based catalyst [57,58].

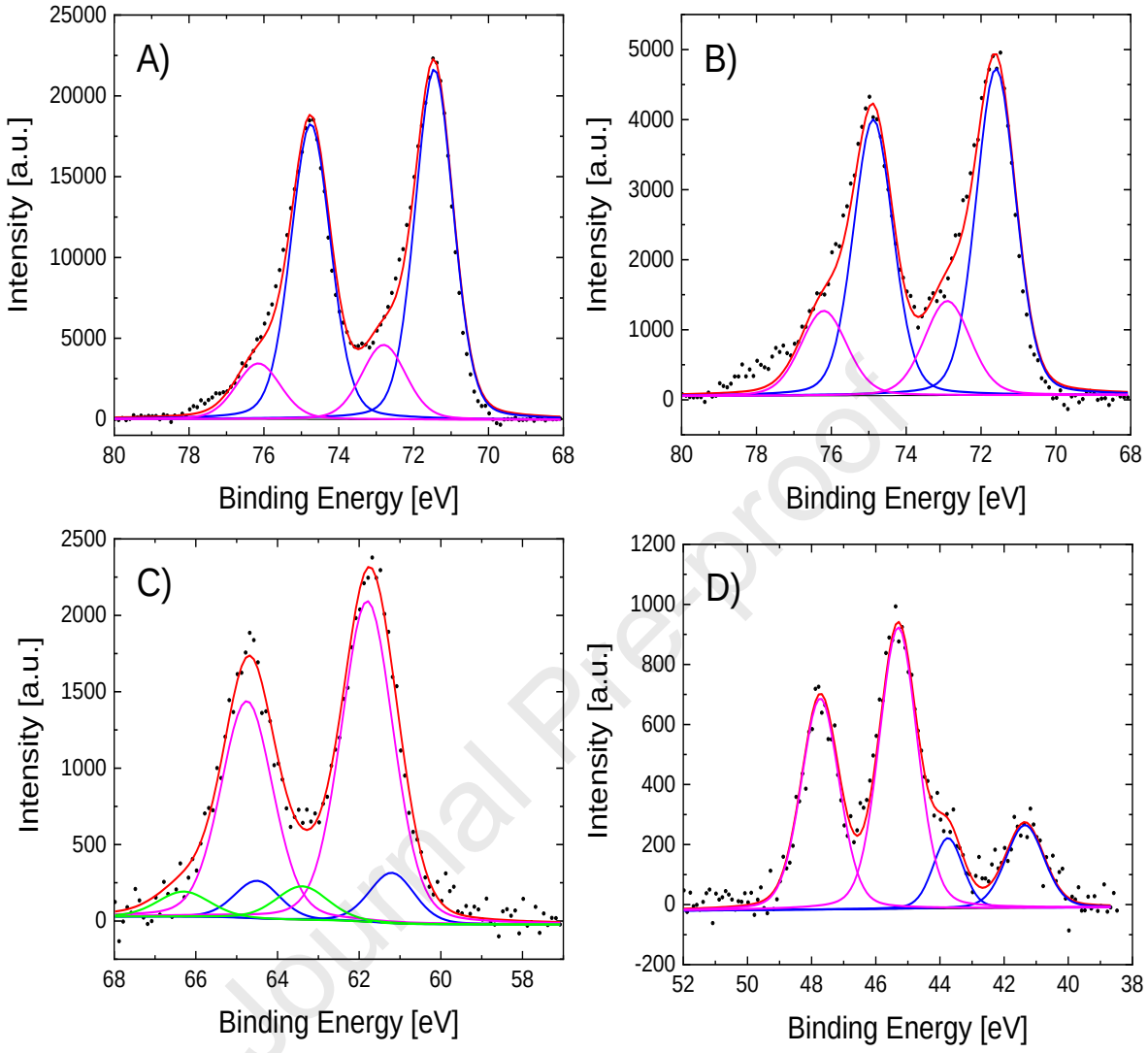

Figure 5. XPS spectrum for bimetallic catalyst synthetized with a PVP/Pt ratio of 1.0: A) Pt4f for Pt/Ir/CB-1 catalyst, B) Pt4f for Pt/Re/CB-1 catalyst, C) Ir4f for Pt/Ir/CB-1 catalyst and D) Ret4f for Pt/Re/CB-1 catalyst.

Ir4f XPS spectra for Pt/Ir/CB catalyst (Figure 5-C) shows 3 doublets with the main peaks at around 61.2, 61.8 and 63.4 eV corresponding to the contributions of Ir^{0}, Ir^{3+} and Ir^{4+}, respectively [59,60]. Interestingly, iridium species present a slight shifting to higher binding energies, which can be associated to the close interaction with Pt, which leads to an electron transfer from Ir to Pt, which proves the formation of Pt/Ir alloys [17,58]. Figure 5-D shows the Re4f XPS spectrum for Pt/Re/CB-1 catalyst, in which two doublets at 41.3 and 45.3 eV are observed associated to Re0

and Re^{6+}, respectively [19,61]. Then, it can be observed that oxidized species (Re^{6+}) is the predominant contribution in the bimetallic catalysts. However, the stability of the zerovalent rhenium species is achieved by the use of PVP during the synthesis, as it is observed for the Pt/Re/CB-1 catalyst. Additionally, Re4f core-level shift towards higher binding energies can be appreciated for the Re^0 species in the Pt/Re/CB-1 catalyst, in comparison with previously studied Re^0 [62]. This may be possibly caused by the electron withdrawing effect from the interaction with Pt in the alloy. It is important to remark that this behavior is eventually more notorious in rhenium than iridium species taking into account the differences of electronegativity between Re and Pt, in comparison with Ir and Pt.

Morphological analysis by TEM in Figure 6 for the bimetallic catalysts shows the presence of spherical nanoparticles that are well-distributed on the CB support when PVP is used, in agreement with previous results in the monometallic catalyst.

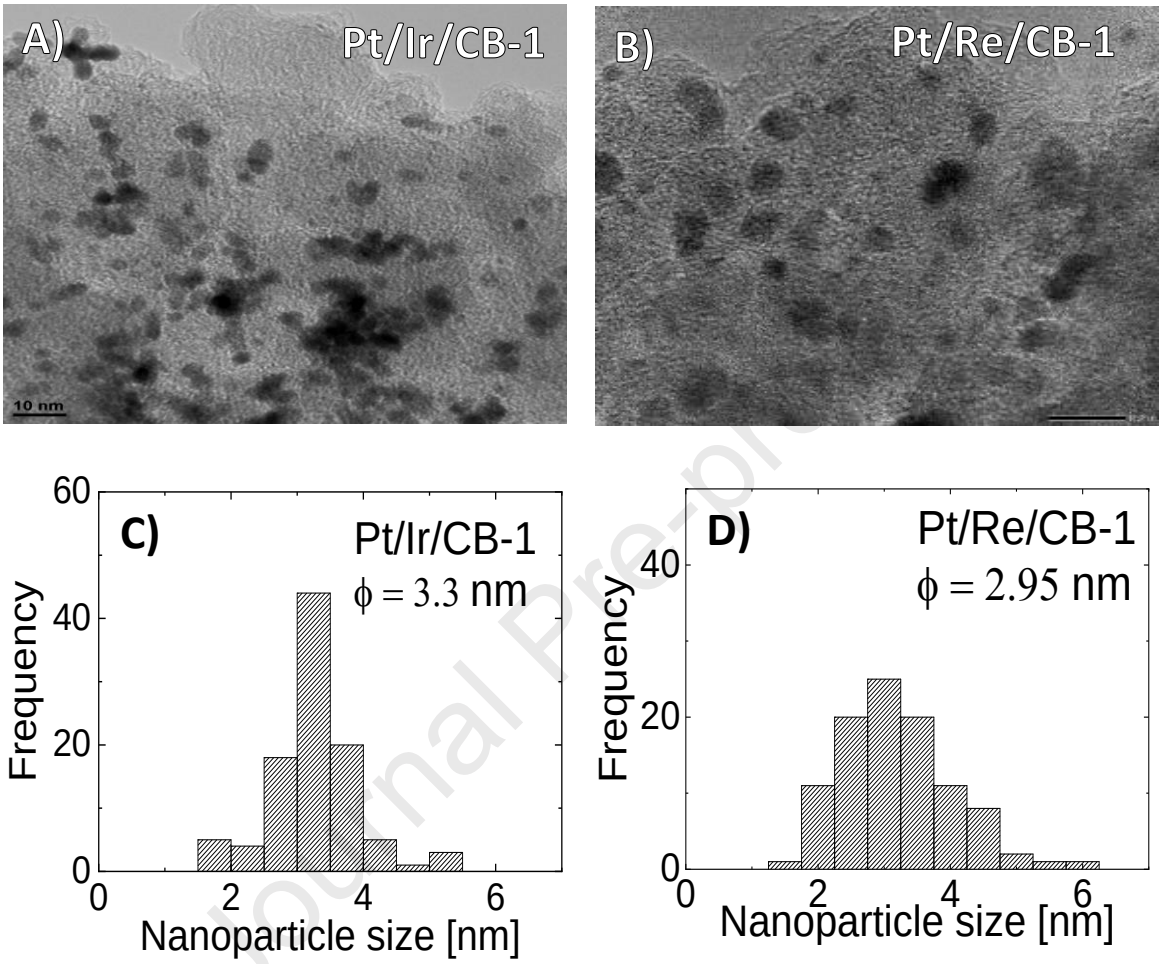

Figure 6. TEM micrographs of A) Pt/Ir/CB-1 and B) Pt/Re/CB-1 bimetallic catalysts synthesized with a PVP/Pt ratio of 1, C) histogram of particle size distribution on Pt/Ir/CB-1 and D) histogram of particle size distribution on Pt/Re/CB-1.

Interestingly, analysis of the nanoparticles shows that the spherical morphology of nanoparticles is maintained and no observable segregation are appreciated, indicating that the Re and Ir are incorporated into the Pt nanoparticles as a single phase. However, some differences are observed among Re and Ir-containing catalysts. Thus, in the case of Ir the degree of aggregation seems to be somewhat higher than for the Pt/CB-1 and Pt/Re/CB-1 catalysts. This makes that the particle size increases in the Pt/Ir/CB-1 catalyst in comparison to the Pt/Re/CB-1 and Pt/CB-1 catalysts (see Figure 6, Table 2 and Table 4).

Electrochemical characterization by cyclic voltammetry of the bimetallic catalysts is presented in Figure 7.

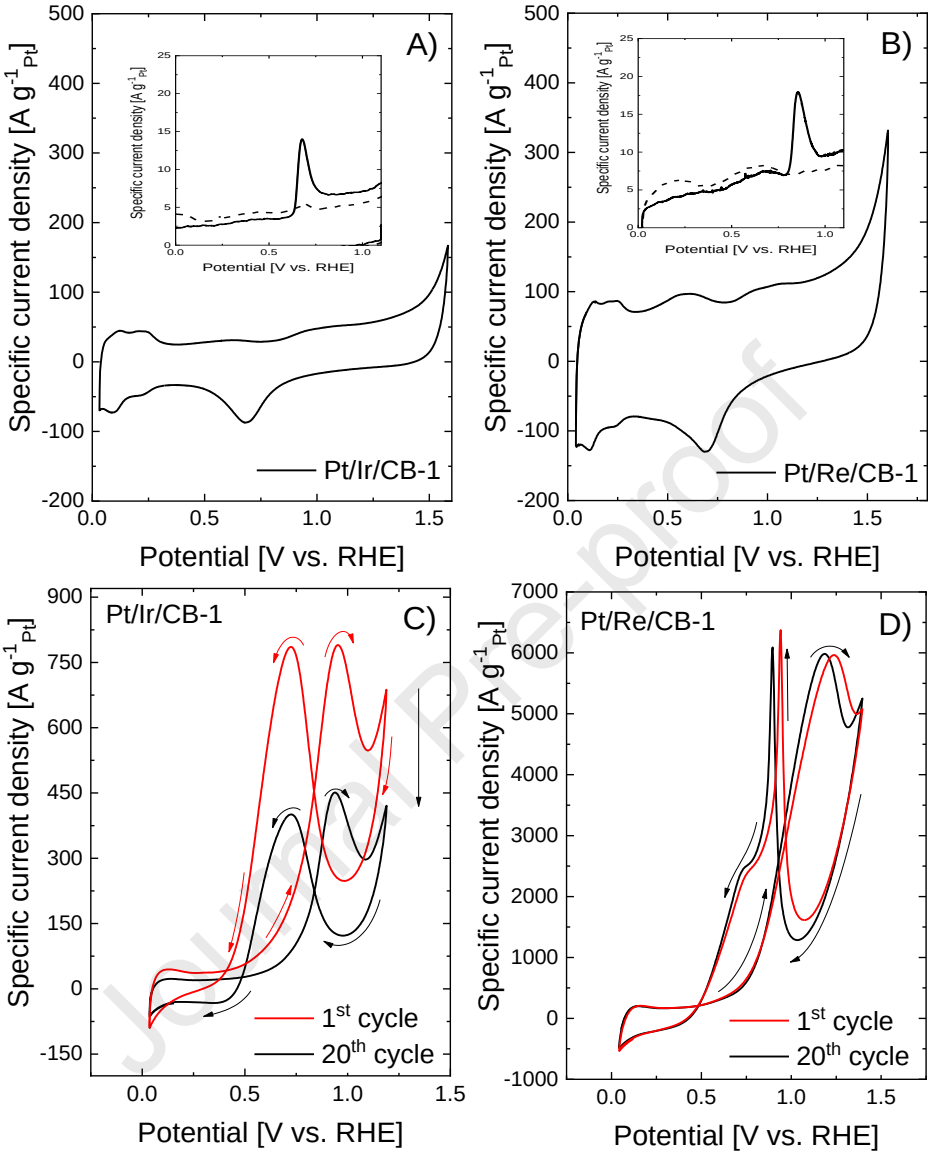

Figure 7. Cyclic voltammograms of bimetallic catalyst: A) Pt/Ir/CB-1 and B) Pt/Re/CB-1 synthesized in 0.5 M H_2SO_4 at 50 mV s^{-1} under inert atmosphere. Inset: CO-stripping profiles performed in 0.5 M H_2SO_4 at 25 mV s^{-1}. Electrocatalytic activity evaluation towards ethanol oxidation of C) Pt/Ir/CB-1 and D) Pt/Re/CB-1 synthesized in 0.5 M H_2SO_4 + 1 M EtOH at 20 mV s^{-1} under inert atmosphere.

In all the bimetallic catalysts, stable cyclic voltammograms show the hydrogen adsorption/desorption region between 0.05 and 0.4 V and the redox processes associated with the oxidation and reduction of Pt at potentials higher than 0.4 V. However, charge contributions of

the hydrogen region in the bimetallic catalyst are attenuated by the presence of the second metal. Furthermore, Pt/Re/CB-1 catalyst presents a more significant decrease in the hydrogen region, in contrast with the Pt/Ir/CB-1 catalyst. This agrees with the results found for Re in the same electrolyte, in which the voltammograms do not present redox processes associated to hydrogen adsorption-desorption in comparison to Ir [63–65].

Then, in Pt/Re/CB-1 in comparison with Pt/CB-1 and Pt/Ir/CB-1 catalysts, the differences observed in the voltammograms are mainly a consequence of a metal oxide layer generated by the second metal during cycling [66]. In this case, rhenium presents a higher tendency to produce this kind of species, similar to what is observed for Sn species [66,67]. Interestingly, the ECSA in the bimetallic catalysts in acid media demonstrated that Pt/Re/CB-1 shows a slight decrease ($ECSA_{Pt/Re/CB-1}$ = 98.3 m^2 g^{-1}), in comparison with the value obtained in the monometallic catalyst (Table 2). In contrast, incorporation of iridium tends to reduce the ECSA to values at around 61.9 m^2 g^{-1}, which might be related to the presence of aggregated nanoparticles, which would cause a reduction of the active area, in comparison with Pt/Re/CB-1 which shows isolated nanoparticles on the support. These results are in agreement with the TEM observations already discussed.

The electrocatalytic activity towards ethanol oxidation of both bimetallic catalysts presented in Figure 7-C and 7-D shows the typical double irreversible wave for the oxidation of EtOH, associated with the primary alcohol oxidation and the oxidative desorption of the CO_{ads} and intermediate species generated at 0.9 and 1.05 V for Pt/Ir and Pt/Re, respectively, in the first wave [68,69]. In case of Pt/Ir/CB-1 no important changes are observed in the electrocatalytic activity in comparison with monometallic catalyst (See Figure S5 in supporting information), in fact, a decrease of the catalytic current density and stability are observed. Additionally, shifting to higher positive potentials of the on-set potential reaction for the forward wave and an important decrease of the current density after cycling might suggest that this catalyst suffers from poisoning by reaction intermediates strongly adsorbed on the surface.

On the other hand, Pt/Re/CB-1 electrode shows a much higher oxidation current density in comparison with the other catalysts (Table 2 and Table 4), which cannot only be explained by the values of ECSA, since these are similar to the monometallic catalysts.

Table 4. Values of ECSA and nanoparticle size for the bimetallic catalyst prepared with a PVP/Pt= 1.

Catalyst	ECSA [$m^2\ g^{-1}$]	d_{ECSA} [nm]	d_{TEM} [nm]	E_{onset} [V]	I_f [A g_{Pt}^{-1}]*	I_f/I_b*
Pt/Ir/CB-1	61.9	4.5	3.30	0.49	342.1	1.12
Pt/Re/CB-1	98.3	2.8	2.95	0.46	5969	0.98

*I_f: current density in the forward wave. I_b: current density in the backward wave. Ratio I_f/I_b was determined in the last cycle.

The presence of oxidized Re species forming an oxide layer may produce an important modification of the electronic properties of active sites. In the backward scan, two irreversible oxidation peaks to about 0.73 and 0.94 V suggest that the oxidation of two different species is taking place in this electrocatalyst together with the direct oxidation of ethanol. However, these two oxidation peaks could be also associated to the oxidation of ethanol in two different catalytic sites. In addition, this electrocatalyst does not exhibit any decrease in the oxidation current density with cycling and a shift to more positive potentials from the on-set potential reaction, suggesting a high tolerance towards poisoning and an outstanding stability after cycling in presence of ethanol.

Even though Re has been reported to favour C-C bond breakdown [26], Re incorporation has not resulted in a direct enhancement in the catalytic activity towards the oxidation of ethanol. In fact, the increase of the peak potential of the forward wave from 0.94 V for Pt and Pt/Ir catalyst to 1.2 V for Pt/Re catalyst suggests that Re might affect the nature of the active sites for adsorption of ethanol as a consequence of a hindrance effect due to the presence of ReO_x and OH_{ads} species [18,24,63], in agreement with other Pt-based alloys [10]. Low loadings of Re in this catalyst possibly may not directly promote the C-C bond breaking in ethanol. However, Re might facilitate

the rupture/release of the intermediates, promoting the oxidative desorption over the Pt surface [24]. In the literature, a significant number of alloying metals (Me: Sn, Re, Ir) have been reported to generate MeO_x and OH_{ads} species from water dissociation which are involved in the removal of the intermediates and adsorbed CO on Pt, providing the poisoning tolerance [17,18,21]. Indeed, part of the OH_{ads} species can be generated prior to ethanol oxidation [57], then once electrooxidation of ethanol takes place on the Pt/Re/CB-1 electrode the CO_{ads} and other intermediates can react in the reverse wave paving the way for the irreversible oxidation and desorption processes observed at a potential of 0.94 V.

In order to conclude the analysis of the optimal electrocatalyst, Figure 8 shows the chronoamperometric profiles performed at 1.0 V for 180 min in presence of EtOH.

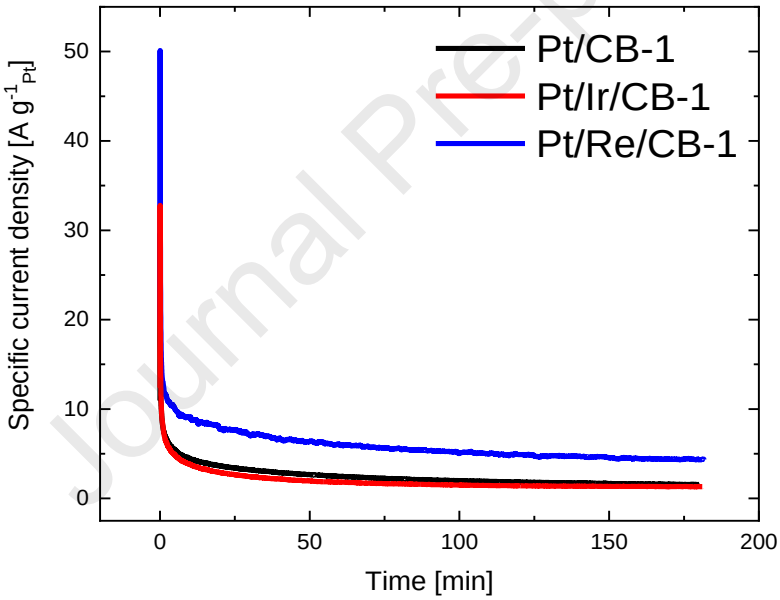

Figure 8. Chronoamperometric profiles of the electrooxidation of ethanol for the optimal mono- and bimetallic Pt-based catalyst. Experiment conducted at 1.0 V in 0.5 M H_2SO_4 + 1 M EtOH.

The current variation in presence of ethanol shows that, the electrocatalyst Pt/CB-1 and Pt/Ir/CB-1 present a clear deactivation of the catalytic activity due to the not completely suppression of the C1 and C2 intermediates adsorbed on surface, in agreement with the CV profiles in Figure 7 and Figure S2. However, current density of the bimetallic electrocatalyst Pt/Re/CB-1 is essentially *ca.* 3 times higher than the other electrocatalyst in presence of ethanol, showing remarkable durability [70]. Then, deactivation degree in this electrocatalyst is lower than

the mono- and Ir/Pt bimetallic catalyst, thus ethanol oxidation is not suppressed in Pt/Re/CB-1 electrocatalyst by the OH_{ads} species generated for the Re species. Comparison of the most relevant electrochemical parameters (see Table S1 in supporting information) demonstrate that the Pt/Re/CB-1 electrocatalyst performance is similar to those reported in literature. Interestingly, the faradic contribution in the forward scan, which is stable after continuous cycling, is highly superior in comparison with the other electrocatalyst, indicative of the stability of the electrocatalyst.

4. Conclusion

Monometallic electrocatalysts (Pt/CB) prepared with different PVP/Pt ratios show the characteristic irreversible oxidation processes associated with the oxidation of ethanol in acid medium. The amount of PVP used during nanoparticle synthesis determined the electrochemical behavior of the resulting catalysts. Catalysts prepared with a PVP/Pt ratio of 2.5 and 10 present no hydrogen adsorption/desorption capability and also a low catalytic activity towards ethanol oxidation, as a consequence of the partial blocking of the active sites in the Pt nanoparticles. These electrocatalysts show a low poisoning tolerance with a high tendency towards poisoning. Therefore, accumulation of the carbon intermediates is more favorable in those electrocatalysts.

Electrocatalysts prepared with smaller PVP/Pt ratios, in which the surface of the Pt nanoparticles is not completely blocked by PVP, show a better performance towards ethanol electrooxidation. Catalyst Pt/CB-1 shows a combination of metal loading and nanoparticle size distribution which provides an optimal value where a high catalytic response is obtained by the high value of ECSA in this catalyst. The bimetallic catalysts can be successfully prepared with a PVP/Pt ratio of 1, producing catalysts in which Pt/Re and Pt/Ir alloys are formed. The incorporation of the second metal produces important changes in the electrocatalytic properties. Electrocatalyst Pt/Re/CB-1 does not show important changes in the ECSA (98.3 $m^2\ g^{-1}$), in comparison with the monometallic catalyst, despite the presence of the second metal. Unlike the catalyst prepared with iridium, in which decreasing of the EASA to values at around 61.9 $m^2\ g^{-1}$

can be related to some nanoparticle aggregation. Interestingly, the presence of rhenium in the alloy promotes bond breaking of the intermediates adsorbed on surface, facilitating its release from the Pt surface. This minimizes catalyst poisoning and results in a highly stable catalyst with no appreciable deactivation with cycling.

Acknowledgements

N. S. V. and G. M. thank to ANPCyT and CONICET for the financial support. A.F.Q.J. gratefully acknowledges Generalitat Valenciana for the financial support through Santiago Grisolia grant (GRISOLIA/2016/084). MICIN and FEDER are acknowledged (projects PIB2019-105923RB-I00 and RTI2018-095291-B-I00).

5. References

[1] B.C.H. Steele, A. Heinzel, Materials for fuel-cell technologies, Nature. 414 (2001) 345–352. https://doi.org/10.1038/35104620.

[2] Y. Wang, K.S. Chen, J. Mishler, S.C. Cho, X.C. Adroher, A review of polymer electrolyte membrane fuel cells: Technology, applications, and needs on fundamental research, Appl. Energy. 88 (2011) 981–1007. https://doi.org/https://doi.org/10.1016/j.apenergy.2010.09.030.

[3] C. Lamy, S. Rousseau, E.M. Belgsir, C. Coutanceau, J.-M. Léger, Recent progress in the direct ethanol fuel cell: development of new platinum–tin electrocatalysts, Electrochim. Acta. 49 (2004) 3901–3908. https://doi.org/https://doi.org/10.1016/j.electacta.2004.01.078.

[4] C. Lamy, A. Lima, V. LeRhun, F. Delime, C. Coutanceau, J.-M. Léger, Recent advances in the development of direct alcohol fuel cells (DAFC), J. Power Sources. 105 (2002) 283–296. https://doi.org/https://doi.org/10.1016/S0378-7753(01)00954-5.

[5] Lamy, C. Leger, J. M, Les piles à combustible : application au véhicule électrique, J. Phys.

IV. 04, C1 (1994) 253-281. https://doi.org/10.1051/jp4:1994119.

[6] J. Tayal, B. Rawat, S. Basu, Bi-metallic and tri-metallic Pt–Sn/C, Pt–Ir/C, Pt–Ir–Sn/C catalysts for electro-oxidation of ethanol in direct ethanol fuel cell, Int. J. Hydrogen Energy. 36 (2011) 14884–14897. https://doi.org/https://doi.org/10.1016/j.ijhydene.2011.03.035.

[7] K. Wang, F. Wang, Y. Zhao, W. Zhang, Surface-tailored PtPdCu ultrathin nanowires as advanced electrocatalysts for ethanol oxidation and oxygen reduction reaction in direct ethanol fuel cell, J. Energy Chem. 52 (2021) 251–261. https://doi.org/https://doi.org/10.1016/j.jechem.2020.04.056.

[8] Wang, Y. Zou, S. Cai, W. B. Recent Advances on Electro-Oxidation of Ethanol on Pt- and Pd-Based Catalysts: From Reaction Mechanisms to Catalytic Materials, Catalysts 5 (2015), 1507-1534. https://doi.org/10.3390/catal5031507.

[9] T. Iwasita, E. Pastor, A dems and FTIR spectroscopic investigation of adsorbed ethanol on polycrystalline platinum, Electrochim. Acta. 39 (1994) 531–537. https://doi.org/https://doi.org/10.1016/0013-4686(94)80097-9.

[10] N.S. Veizaga, V.A. Paganin, T.A. Rocha, O.A. Scelza, S.R. de Miguel, E.R. Gonzalez, Development of PtGe and PtIn anodic catalysts supported on carbonaceous materials for DMFC, Int. J. Hydrogen Energy. 39 (2014) 8728–8737. https://doi.org/https://doi.org/10.1016/j.ijhydene.2013.12.041.

[11] W.J. Zhou, S.Q. Song, W.Z. Li, Z.H. Zhou, G.Q. Sun, Q. Xin, S. Douvartzides, P. Tsiakaras, Direct ethanol fuel cells based on PtSn anodes: the effect of Sn content on the fuel cell performance, J. Power Sources. 140 (2005) 50–58. https://doi.org/https://doi.org/10.1016/j.jpowsour.2004.08.003.

[12] L. Dubau, F. Hahn, C. Coutanceau, J.-M. Léger, C. Lamy, On the structure effects of

bimetallic PtRu electrocatalysts towards methanol oxidation, J. Electroanal. Chem. 554–555 (2003) 407–415. https://doi.org/https://doi.org/10.1016/S0022-0728(03)00308-5.

[13] M.-S. Löffler, H. Natter, R. Hempelmann, K. Wippermann, Preparation and characterisation of Pt–Ru model electrodes for the direct methanol fuel cell, Electrochim. Acta. 48 (2003) 3047–3051. https://doi.org/https://doi.org/10.1016/S0013-4686(03)00375-X.

[14] W. Li, W. Zhou, H. Li, Z. Zhou, B. Zhou, G. Sun, Q. Xin, Nano-stuctured Pt–Fe/C as cathode catalyst in direct methanol fuel cell, Electrochim. Acta. 49 (2004) 1045–1055. https://doi.org/https://doi.org/10.1016/j.electacta.2003.10.015.

[15] N.S. Veizaga, V.I. Rodriguez, T.A. Rocha, M. Bruno, O.A. Scelza, S.R. de Miguel, E.R. Gonzalez, Promoting Effect of Tin in Platinum Electrocatalysts for Direct Methanol Fuel Cells (DMFC), J. Electrochem. Soc. 162 (2014) F243–F249. https://doi.org/10.1149/2.0181503jes.

[16] M. Götz, H. Wendt, Binary and ternary anode catalyst formulations including the elements W, Sn and Mo for PEMFCs operated on methanol or reformate gas, Electrochim. Acta. 43 (1998) 3637–3644. https://doi.org/https://doi.org/10.1016/S0013-4686(98)00121-2.

[17] W. Chen, S. Chen, Iridium-platinum alloy nanoparticles: Composition-dependent electrocatalytic activity for formic acid oxidation, J. Mater. Chem. 21 (2011) 9169–9178. https://doi.org/10.1039/C1JM00077B.

[18] D. Raciti, J. Kubal, C. Ma, M. Barclay, M. Gonzalez, M. Chi, J. Greeley, K.L. More, C. Wang, Pt_3Re alloy nanoparticles as electrocatalysts for the oxygen reduction reaction, Nano Energy. 20 (2016) 202–211. https://doi.org/https://doi.org/10.1016/j.nanoen.2015.12.014.

[19] H.-D. Kim, H.J. Park, T.-W. Kim, K.-E. Jeong, H.-J. Chae, S.-Y. Jeong, C.-H. Lee, C.-U. Kim, The effect of support and reaction conditions on aqueous phase reforming of polyol

over supported Pt–Re bimetallic catalysts, Catal. Today. 185 (2012) 73–80. https://doi.org/https://doi.org/10.1016/j.cattod.2011.08.012.

[20] T. Sheng, W.-F. Lin, C. Hardacre, P. Hu, Significance of β-dehydrogenation in ethanol electro-oxidation on platinum doped with Ru, Rh, Pd, Os and Ir, Phys. Chem. Chem. Phys. 16 (2014) 13248–13254. https://doi.org/10.1039/C4CP00737A.

[21] S.J. Hwang, S.J. Yoo, T.-Y. Jeon, K.-S. Lee, T.-H. Lim, Y.-E. Sung, S.-K. Kim, Facile synthesis of highly active and stable Pt–Ir/C electrocatalysts for oxygen reduction and liquid fuel oxidation reaction, Chem. Commun. 46 (2010) 8401–8403. https://doi.org/10.1039/C0CC03125A.

[22] Q. Chang, S. Kattel, X. Li, Z. Liang, B.M. Tackett, S.R. Denny, P. Zhang, D. Su, J.G. Chen, Z. Chen, Enhancing C–C Bond Scission for Efficient Ethanol Oxidation using PtIr Nanocube Electrocatalysts, ACS Catal. 9 (2019) 7618–7625. https://doi.org/10.1021/acscatal.9b02039.

[23] M. Li, D.A. Cullen, K. Sasaki, N.S. Marinkovic, K. More, R.R. Adzic, Ternary Electrocatalysts for Oxidizing Ethanol to Carbon Dioxide: Making Ir Capable of Splitting C–C Bond, J. Am. Chem. Soc. 135 (2013) 132–141. https://doi.org/10.1021/ja306384x.

[24] J. Tayal, B. Rawat, S. Basu, Effect of addition of rhenium to Pt-based anode catalysts in electro-oxidation of ethanol in direct ethanol PEM fuel cell, Int. J. Hydrogen Energy. 37 (2012) 4597–4605. https://doi.org/https://doi.org/10.1016/j.ijhydene.2011.05.188.

[25] M. Bonarowska, A. Malinowski, Z. Karpiński, Hydrogenolysis of C–C and C–Cl bonds by Pd–Re/Al_2O_3 catalysts, Appl. Catal. A Gen. 188 (1999) 145–154. https://doi.org/https://doi.org/10.1016/S0926-860X(99)00241-0.

[26] A.K. Aboul-Gheit, M.F. Menoufy, A.K. El-Morsi, Hydroconversion of n-heptane on catalysts containing platinum, rhenium and platinum-rhenium on sodium mordenite, Appl. Catal. 61 (1990) 283–292. https://doi.org/https://doi.org/10.1016/S0166-9834(00)82151-

X.

[27] A.K. Choudhary, H. Pramanik, Addition of rhenium (Re) to Pt-Ru/f-MWCNT anode electrocatalysts for enhancement of ethanol electrooxidation in half cell and single direct ethanol fuel cell, Int. J. Hydrogen Energy. 45 (2020) 13300–13321. https://doi.org/https://doi.org/10.1016/j.ijhydene.2020.03.044.

[28] E. Drzymała, G. Gruzeł, J. Depciuch, M. Pawlyta, M. Donten, M. Parlinska-Wojtan, Ternary Pt/Re/SnO_2/C catalyst for EOR: Electrocatalytic activity and durability enhancement, Nano Res. 13 (2020) 832–842. https://doi.org/10.1007/s12274-020-2704-1.

[29] S. Domínguez-Domínguez, J. Arias-Pardilla, Á. Berenguer-Murcia, E. Morallón, D. Cazorla-Amorós, Electrochemical deposition of platinum nanoparticles on different carbon supports and conducting polymers, J. Appl. Electrochem. 38 (2008) 259–268. https://doi.org/10.1007/s10800-007-9435-9.

[30] J. Zhang, X. Wang, C. Wu, H. Wang, B. Yi, H. Zhang, Preparation and characterization of Pt/C catalysts for PEMFC cathode: effect of different reduction methods, React. Kinet. Catal. Lett. 83 (2004) 229–236. https://doi.org/10.1023/B:REAC.0000046081.96554.ae.

[31] N. Veizaga, J. Fernandez, M. Bruno, O. Scelza, S. de Miguel, Deposition of Pt nanoparticles on different carbonaceous materials by using different preparation methods for PEMFC electrocatalysts, Int. J. Hydrogen Energy. 37 (2012) 17910–17920. https://doi.org/https://doi.org/10.1016/j.ijhydene.2012.08.144.

[32] Y. Zheng, Z. Dou, Y. Fang, M. Li, X. Wu, J. Zeng, Z. Hou, S. Liao, Platinum nanoparticles on carbon-nanotube support prepared by room-temperature reduction with H2 in ethylene glycol/water mixed solvent as catalysts for polymer electrolyte membrane fuel cells, J. Power Sources. 306 (2016) 448–453. https://doi.org/https://doi.org/10.1016/j.jpowsour.2015.12.077.

[33] A. Henglein, M. Giersig, Reduction of Pt(II) by H_2: Effects of Citrate and NaOH and

Reaction Mechanism, J. Phys. Chem. B. 104 (2000) 6767–6772. https://doi.org/10.1021/jp000801o.

[34] F. Fiévet, S. Ammar-Merah, R. Brayner, F. Chau, M. Giraud, F. Mammeri, J. Peron, J.-Y. Piquemal, L. Sicard, G. Viau, The polyol process: a unique method for easy access to metal nanoparticles with tailored sizes, shapes and compositions, Chem. Soc. Rev. 47 (2018) 5187–5233. https://doi.org/10.1039/C7CS00777A.

[35] P. Lu, T. Teranishi, K. Asakura, M. Miyake, N. Toshima, Polymer-Protected Ni/Pd Bimetallic Nano-Clusters: Preparation, Characterization and Catalysis for Hydrogenation of Nitrobenzene, J. Phys. Chem. B. 103 (1999) 9673–9682. https://doi.org/10.1021/jp992177p.

[36] H.J. Salavagione, C. Sanchís, E. Morallón, Friendly Conditions Synthesis of Platinum Nanoparticles Supported on a Conducting Polymer: Methanol Electrooxidation, J. Phys. Chem. C. 111 (2007) 12454–12460. https://doi.org/10.1021/jp071037+.

[37] A. Ortega-Murcia, M. Navlani-García, E. Morallón, D. Cazorla-Amorós, MWCNT-Supported PVP-Capped Pd Nanoparticles as Efficient Catalysts for the Dehydrogenation of Formic Acid, Front. Chem. 8 (2020) 359. https://doi.org/10.3389/fchem.2020.00359.

[38] A. Gabe, J. García-Aguilar, Á. Berenguer-Murcia, E. Morallón, D. Cazorla-Amorós, Key factors improving oxygen reduction reaction activity in cobalt nanoparticles modified carbon nanotubes, Appl. Catal. B Environ. 217 (2017) 303–312. https://doi.org/https://doi.org/10.1016/j.apcatb.2017.05.096.

[39] P. Navarro-Botella, J. García-Aguilar, Á. Berenguer-Murcia, D. Cazorla-Amorós, Pd and Cu-Pd nanoparticles supported on multiwall carbon nanotubes for H_2 detection, Mater. Res. Bull. 93 (2017) 102–111. https://doi.org/https://doi.org/10.1016/j.materresbull.2017.04.040.

[40] A.F. Quintero-Jaime, Á. Berenguer-Murcia, D. Cazorla-Amorós, E. Morallón, Carbon

Nanotubes Modified With Au for Electrochemical Detection of Prostate Specific Antigen: Effect of Au Nanoparticle Size Distribution, Front. Chem. 7 (2019) 147. https://doi.org/10.3389/fchem.2019.00147.

[41] S. Domínguez-Domínguez, Á. Berenguer-Murcia, D. Cazorla-Amorós, Á. Linares-Solano, Semihydrogenation of phenylacetylene catalyzed by metallic nanoparticles containing noble metals, J. Catal. 243 (2006) 74–81. https://doi.org/10.1016/j.jcat.2006.06.027.

[42] V.I. Rodríguez, N.S. Veizaga, S.R. de Miguel, Effect of the Preparation Method on the Electrocatalytic Activity of Pt-Sn/Nanotubes Catalysts Used in DMFC, J. Electrochem. Soc. 164 (2017) F1524–F1533. https://doi.org/10.1149/2.1811713jes.

[43] J. V Rojas, C.H. Castano, Synthesis of rhenium oxide nanoparticles (Re_xO_y) by gamma irradiation, Radiat. Phys. Chem. 99 (2014) 1–5. https://doi.org/https://doi.org/10.1016/j.radphyschem.2014.01.022.

[44] K. Baranowska, J. Okal, W. Tylus, Microwave-assisted polyol synthesis of bimetallic RuRe nanoparticles stabilized by PVP or oxide supports (γ-alumina and silica), Appl. Catal. A Gen. 511 (2016) 117–130. https://doi.org/https://doi.org/10.1016/j.apcata.2015.11.045.

[45] D.G. Castner, K. Hinds, D.W. Grainger, X-ray Photoelectron Spectroscopy Sulfur 2p Study of Organic Thiol and Disulfide Binding Interactions with Gold Surfaces, Langmuir. 12 (1996) 5083–5086. https://doi.org/10.1021/la960465w.

[46] M. Chen, Y. Xing, Polymer-Mediated Synthesis of Highly Dispersed Pt Nanoparticles on Carbon Black, Langmuir. 21 (2005) 9334–9338. https://doi.org/10.1021/la051892p.

[47] A. Sukeri, L. P. H. Saravia, M. Bertotti, A Facile Electrochemical Approach to Fabricate a Nanoporous Gold Film Electrode and its Electrocatalytic Activity Towards Dissolved Oxygen Reduction. Phys. Chem. Chem. Phys. 17 (2015) 28510–28514.

https://doi.org/10.1039/C5CP05220C

[48] J. García-Aguilar, M. Navlani-García, Á. Berenguer-Murcia, K. Mori, Y. Kuwahara, H. Yamashita, D. Cazorla-Amorós, Evolution of the PVP–Pd Surface Interaction in Nanoparticles through the Case Study of Formic Acid Decomposition, Langmuir. 32 (2016) 12110–12118. https://doi.org/10.1021/acs.langmuir.6b03149.

[49] I. Miguel-García, Á. Berenguer-Murcia, T. García, D. Cazorla-Amorós, Effect of the aging time of PVP coated palladium nanoparticles colloidal suspensions on their catalytic activity in the preferential oxidation of CO, Catal. Today. 187 (2012) 2–9. https://doi.org/https://doi.org/10.1016/j.cattod.2012.02.015.

[50] I. Miguel-García, Á. Berenguer-Murcia, D. Cazorla-Amorós, Preferential oxidation of CO catalyzed by supported polymer-protected palladium-based nanoparticles, Appl. Catal. B Environ. 98 (2010) 161–170. https://doi.org/10.1016/j.apcatb.2010.05.025.

[51] H. Bönnemann, R.M. Richards, Nanoscopic Metal Particles − Synthetic Methods and Potential Applications, Eur. J. Inorg. Chem. 2001 (2001) 2455–2480. https://doi.org/10.1002/1099-0682(200109)2001:10<2455::AID-EJIC2455>3.0.CO;2-Z.

[52] A. Sukeri, L.P.H. Saravia, M. Bertotti, A facile electrochemical approach to fabricate a nanoporous gold film electrode and its electrocatalytic activity towards dissolved oxygen reduction, Phys. Chem. Chem. Phys. 17 (2015) 28510–28514. https://doi.org/10.1039/C5CP05220C.

[53] F. Zaragoza-Martín, D. Sopeña-Escario, E. Morallón, C.S.M. de Lecea, Pt/carbon nanofibers electrocatalysts for fuel cells. Effect of the support oxidizing treatment, J. Power Sources. 171 (2007) 302–309. https://doi.org/10.1016/j.jpowsour.2007.06.078.

[54] R.M. Antoniassi, H. Erikson, J. Solla-Gullón, R.M. Torresi, J.M. Feliu, Formic acid electrooxidation on small, {100} structured, and Pd decorated carbon-supported Pt nanoparticles, J. Catal. 400 (2021) 140–147.

https://doi.org/https://doi.org/10.1016/j.jcat.2021.05.026.

[55] A. López-Cudero, J. Solla-Gullón, E. Herrero, A. Aldaz, J.M. Feliu, CO electrooxidation on carbon supported platinum nanoparticles: Effect of aggregation, J. Electroanal. Chem. 644 (2010) 117–126. https://doi.org/https://doi.org/10.1016/j.jelechem.2009.06.016.

[56] Z. Liu, X.Y. Ling, X. Su, J.Y. Lee, Carbon-Supported Pt and PtRu Nanoparticles as Catalysts for a Direct Methanol Fuel Cell, J. Phys. Chem. B. 108 (2004) 8234–8240. https://doi.org/10.1021/jp049422b.

[57] S. Beyhan, C. Coutanceau, J.-M. Léger, T.W. Napporn, F. Kadırgan, Promising anode candidates for direct ethanol fuel cell: Carbon supported PtSn-based trimetallic catalysts prepared by Bönnemann method, Int. J. Hydrogen Energy. 38 (2013) 6830–6841. https://doi.org/https://doi.org/10.1016/j.ijhydene.2013.03.058.

[58] B. Sen, A. Aygun, A. Şavk, M.H. Çalımlı, M.F. Fellah, F. Sen, Composites of Platinum-Iridium Alloy Nanoparticles and GrapheneOxide for the Dimethyl Amine Borane (DMAB) dehydrogenation at ambient conditions: An Experimental and Density Functional Theory Study, Sci. Rep. 9 (2019) 15543. https://doi.org/10.1038/s41598-019-52038-3.

[59] NIST X-ray Photoelectron Spectroscopy Database, NIST Standard Reference Database Number 20, National Institute of Standards and Technology, Gaithersburg MD, 20899 (2000), (https://srdata.nist.gov/xps/EngElmSrchQuery.aspx?EType=PE&CSOpt=Retri_ex_dat&Elm=Ir [Accessed 2020 August 10]).

[60] M. Hara, K. Asami, K. Hashimoto, T. Masumoto, An X-ray photoelectron spectroscopic study of electrocatalytic activity of platinum group metals for chlorine evolution, Electrochim. Acta. 28 (1983) 1073–1081. https://doi.org/https://doi.org/10.1016/0013-4686(83)80011-5.

[61] NIST X-ray Photoelectron Spectroscopy Database, NIST Standard Reference Database Number 20, National Institute of Standards and Technology, Gaithersburg MD, 20899 (2000), (https://srdata.nist.gov/xps/EngElmSrchQuery.aspx?EType=PE&CSOpt=Retri_ex_dat&Elm=Re [Accessed 2020 October 10]).

[62] A.S.Y. Chan, G.K. Wertheim, H. Wang, M.D. Ulrich, J.E. Rowe, T.E. Madey, Surface atom core-level shifts of clean and oxygen-covered Re, Phys. Rev. B. 72 (2005) 35442. https://doi.org/10.1103/PhysRevB.72.035442.

[63] S. Koh, P. Strasser, Electrocatalysis on Bimetallic Surfaces: Modifying Catalytic Reactivity for Oxygen Reduction by Voltammetric Surface Dealloying, J. Am. Chem. Soc. 129 (2007) 12624–12625. https://doi.org/10.1021/ja0742784.

[64] J.O. Zerbino, N.R. de Tacconi, A.J. Arvía, The Activation and Deactivation of Iridium Electrodes in Acid Electrolytes, J. Electrochem. Soc. 125 (1978) 1266–1276. https://doi.org/10.1149/1.2131661.

[65] D.A.J. Rand, R. Woods, Cyclic voltammetric studies on iridium electrodes in sulphuric acid solutions: Nature of oxygen layer and metal dissolution, J. Electroanal. Chem. Interfacial Electrochem. 55 (1974) 375–381. https://doi.org/https://doi.org/10.1016/S0022-0728(74)80431-6.

[66] K. Juodkazis, J. Juodkazytė, T. Juodienė, V. Šukienė, I. Savickaja, Alternative view of anodic surface oxidation of noble metals, Electrochim. Acta. 51 (2006) 6159–6164. https://doi.org/https://doi.org/10.1016/j.electacta.2006.01.071.

[67] J. Ribeiro, D.M. dos Anjos, K.B. Kokoh, C. Coutanceau, J.-M. Léger, P. Olivi, A.R. de Andrade, G. Tremiliosi-Filho, Carbon-supported ternary PtSnIr catalysts for direct ethanol fuel cell, Electrochim. Acta. 52 (2007) 6997–7006. https://doi.org/https://doi.org/10.1016/j.electacta.2007.05.017.

[68] Y. Xu, A. Amini, M. Schell, Mechanistic explanation for a subharmonic bifurcation and variations in behaviour in the voltammetric oxidations of ethanol, 1-propanol and 1-butanol, J. Electroanal. Chem. 398 (1995) 95–104. https://doi.org/https://doi.org/10.1016/0022-0728(95)04227-6.

[69] L.W.H. Leung, M.J. Weaver, Real-time FTIR spectroscopy as a quantitative kinetic probe of competing electrooxidation pathways of small organic molecules, J. Phys. Chem. 92 (1988) 4019–4022. https://doi.org/10.1021/j100325a004.

[70] R. Rizo, R.M. Arán-Ais, E. Padgett, D.A. Muller, M.J. Lázaro, J. Solla-Gullón, J.M. Feliu, E. Pastor, H.D. Abruña, Pt-Richcore/Sn-Richsubsurface/Ptskin Nanocubes As Highly Active and Stable Electrocatalysts for the Ethanol Oxidation Reaction, J. Am. Chem. Soc. 140 (2018) 3791–3797. https://doi.org/10.1021/jacs.8b00588.

- Mono- and bimetallic electrocatalyst for ethanol oxidation reaction.
- Controlled amount and electrochemical active surface area of Pt in mono- and bimetallic by the synthesis of electrocatalyst.
- High CO-tolerance of electrocatalyst with small addition of Re.

Declaration of interests

☒ The authors declare that they have no known competing financial interests or personal relationships that could have appeared to influence the work reported in this paper.

☐The authors declare the following financial interests/personal relationships which may be considered as potential competing interests: